SCIENCE CHINA
Information Sciences

• RESEARCH PAPER •

November 2019, Vol. 62 212204:1–212204:17
https://doi.org/10.1007/s11432-018-9887-5

# Coordinated flight control of miniature fixed-wing UAV swarms: methods and experiments

Xiangke WANG[1], Lincheng SHEN[1*], Zhihong LIU[1], Shulong ZHAO[1], Yirui CONG[1], Zhongkui LI[2], Shengde JIA[1], Hao CHEN[1], Yangguan YU[1], Yuan CHANG[1] & Yajing WANG[1]

[1]*College of Mechantronics and Automation, National University of Defense Technology, Changsha* 410073*, China;*
[2]*College of Engineering, Peking University, Beijing* 100871*, China*

Received 9 November 2018/Revised 3 February 2019/Accepted 29 March 2019/Published online 19 September 2019

**Abstract** In this paper, we present our recent advances in both theoretical methods and field experiments for the coordinated control of miniature fixed-wing unmanned aerial vehicle (UAV) swarms. We propose a multi-layered group-based architecture, which is modularized, mission-oriented, and can implement large-scale swarms. To accomplish the desired coordinated formation flight, we present a novel distributed coordinated-control scheme comprising a consensus-based circling rendezvous, a coordinated path-following control for the leader UAVs, and a leader-follower coordinated control for the follower UAVs. The current framework embeds a formation pattern reconfiguration technique. Moreover, we discuss two security solutions (inter-UAV collision avoidance and obstacle avoidance) in the swarm flight problem. The effectiveness of the proposed coordinated control methods was demonstrated in field experiments by deploying up to 21 fixed-wing UAVs.

**Keywords** unmanned aerial vehicle, cooperative control, formation control, distributed control, multi-agent system

**Citation** Wang X K, Shen L C, Liu Z H, et al. Coordinated flight control of miniature fixed-wing UAV swarms: methods and experiments. Sci China Inf Sci, 2019, 62(11): 212204, https://doi.org/10.1007/s11432-018-9887-5

## 1 Introduction

Under coordinated control, a group of unmanned aerial vehicles (UAVs) can accomplish a common objective in civilian or military missions such as formation flying [1, 2], cooperative surveillance and searching [3, 4], cooperative transport [5], cooperative task allocation [6], and cooperative path planning [7,8]. A collaborative team of UAVs can more effectively accomplish complex tasks compared to an individual UAV. Other distinct advantages of cooperative UAVs are reduced cost, redundancy handling, and increased maneuverability and robustness [1, 3]. The coordinated control of UAVs requires efficient cooperative control algorithms that generate the prescribed collective behaviors via cooperation among the agents. Considering the limited communication capacity and applicability to large-scale missions comprising many micro UAVs, such cooperative control algorithms are expected to be distributed and depend only on local information sharing among neighboring UAVs that are in close proximity [9–14].

In the last decade, the coordinated control of UAVs in different settings has been studied by many researchers from different perspectives. Wang et al. [15] proposed a leader-follower control law for forming multiple UAVs with obstacle avoidance. Abdessameud and Tayebi [16] presented a consensus-based

* Corresponding author (email: lcshen@nudt.edu.cn)

 

formation controller along with time delays for UAV swarms. A distributed robust cascade-feedback approach that controls the formation and reconfiguration of a team of vertical takeoff and landing (VTOL) UAVs has also been proposed [17]. Zou et al. [18] considered the formation control of a team of VTOL UAVs with uniformly and jointly connected switching topologies. Nigam et al. [19] proposed control policies for the persistent surveillance of multiple UAVs, and tested them in a realistic scenario using two to four quadrotor UAVs. Kushleyev [20] tested time-invariant flight formation by a 20-member team of micro-quadrotors in an indoor environment. Time-varying formation-control problems of multiple quadrotors have also been investigated and tested in outdoor experiments using four quadrotors [21, 22]. The authors of [23] studied the formation control of multiple UAVs in the presence of parametric uncertainties and validated their theoretical results in experiments on three quadrotors. Liu et al. [24] studied the robust formation control of multiple quadrotors subjected to nonlinear dynamics and external disturbances.

Most of the aforementioned studies investigated the cooperative control of multiple quadrotors. However, the cooperative control problem of fixed-wing UAVs becomes much more challenging for at least two reasons. First, unlike quadrotors, fixed-wing UAVs cannot move backwards or stop and are constrained by a minimum forward speed. Second, as fixed-wing UAVs generally fly outdoors, they must be tested in outdoor experiments, which are more demanding than indoor ones and suffer considerably from communication constraints. Consequently, the cooperative control of multiple fixed-wing UAVs has been rarely reported. Among the few existing studies, Xargay et al. [25] described a coordinated path-following approach that controls multiple autonomous vehicles in time-critical missions. The authors of [2] presented a formation control law for a set of fixed-wing research UAVs and tested it on two flying aircrafts. The formation controller in [2] comprises an inner- and outer-loop structure in which the horizontal outer-loop guidance laws are based on nonlinear dynamic inversion. Bayraktar et al. [26] designed a system architecture and an overall system integration for the cooperative control of multiple fixed-wing UAVs and experimentally tested it on two fixed-wing UAVs. By implementing Reynolds flocking rules [27] in a swarm of small fixed-wing flying robots, Hauert et al. [28] coordinated up to 10 airborne robots in outdoor experiments. Recently, live-fly field experiments of 50 fixed-wing UAVs in cooperative autonomous flight operations were reported in [29].

In this study, we present our latest advances on both theoretical algorithms and field experiments for the coordinated control of multiple miniature fixed-wing UAVs. One of our main contributions is a novel hierarchical modularized architecture comprising five top-down layers, namely, human interaction, communication, coordination, high-level, and low-level control layers. This study focuses on the coordination layer, which dynamically divides UAVs into several groups according to the mission requirements and the underlying communication availability. By slicing the overall system into five layers with specified functionalities, our approach significantly reduces the complexity of developing a large-scale swarm system. Unlike the architecture in [29], our architecture is modularized and mission-oriented; therefore, it is conveniently adaptable to the desired missions.

Another main contribution is our distributed coordinated control algorithm, which is composed of three components, namely, a consensus-based circling rendezvous, a coordinated path-following control for the leader UAVs, and a leader-follower coordinated control for the follower UAVs. Under the consensus-based circling law, the UAVs take off successively and prepare for their forthcoming formation mission and provide a safe buffer mechanism against collisions. The coordinated path-following control approach maneuvers the leader UAVs in each group. Moreover, the leader-follower coordination control law guides the follower UAVs along the induced route. The current framework also considers the reconfiguration problem of the formation pattern. The leader UAVs reconfigure the formation by a coordinated path-planning scheme, and the followers simply change their relative positions with respect to their leaders. The coordinated path-following approach of Xargay el al. [25] is similar to ours; however, it adopts a time-parameterized trajectory and ignores the input constraints of fixed-wing UAVs. Our path-following approach considers the geometric path under the prescribed control constraints, which is much easier to implement compared to the prior approach. The current framework also embeds flight security techniques such as collision and obstacle avoidance.

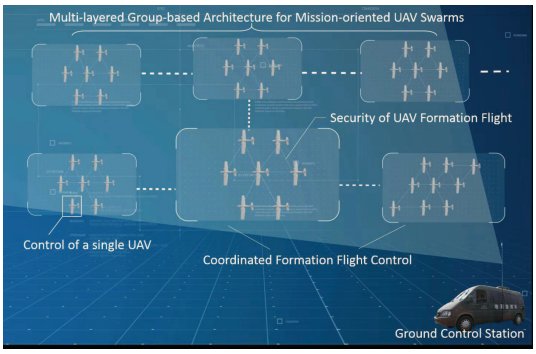


**Figure 1** (Color online) Framework of the overall system.


**Figure 2** (Color online) Snapshot of the overall system.

Our third contribution is the successful completion of field experiments on 21 low-cost fixed-wing UAVs. The UAV team accomplished important missions such as formation maintenance, fast reconfiguration of different formations, and collision and obstacle avoidance. The results demonstrated the effectiveness of the proposed distributed coordination-control algorithms. To the best of the authors knowledge, this is possibly the first demonstration (at least in China) of coordinated formation flying of >20 fixed-wing UAVs under the control of distributed coordination algorithms. Most of the previous studies adopted the individual path-following approach, in which each UAV simply follows the trajectory previously generated by the ground station without sharing its information with other UAVs.

The remainder of this paper is organized as follows. In Section 2, we describe the overall system, whereas in Section 3, we have proposed our multi-layered group-based swarm architecture. In Section 4, we provide a detailed account of our distributed coordinated control algorithm and analyze the results of the field experiments. In Section 5, the security issues of UAV formation flying are investigated. Finally, in Section 6, we provide the conclusion for this study.

## 2 Overall system description

The UAVs deployed for the swarm experiments are identical miniature fixed-wing UAVs (named LINYAN) designed by our team. The approximate wing span and body length of each vehicle are 1800 and 1220 mm, respectively. The approximate cruise airspeed, maximum forward speed, and stall speed are 18, 25, and 8 m/s, respectively. All UAVs are equipped with identical on-board avionics and instrumentation. Each UAV carries the receiver of a global positioning system for self-location and wireless modems for building a communication network with other UAVs.

A number of the miniature fixed-wing UAVs, along with inter-UAV communications, are constructed as a networked swarm system in the air. The ground station is a ground vehicle refitted with the software developed by our team; it is integrated into the overall system by ground-to-air communication. The ground station is operated by a single commander who mainly implemented multi-UAV online trajectory plotting, flight state monitoring, and high-level human command transmission. Thus, the overall system comprises the networked swarm system in the air, the ground station, and the communications. The framework and a real-time snapshot of the overall system are shown in Figures 1 and 2, respectively.

**Remark 1.** Note that the traditional approach that relies on point-to-point connection of each UAV is infeasible for UAV swarms because simultaneous package transmission overwhelms the communication system. The number of communication conflicts would likely increase as more UAVs are deployed. Instead, a latency-sensitive channel based on a mesh networked radio system is developed for inter-UAV communication within swarm systems. In this channel, the UAV can communicate with at most eight nearest neighbors.

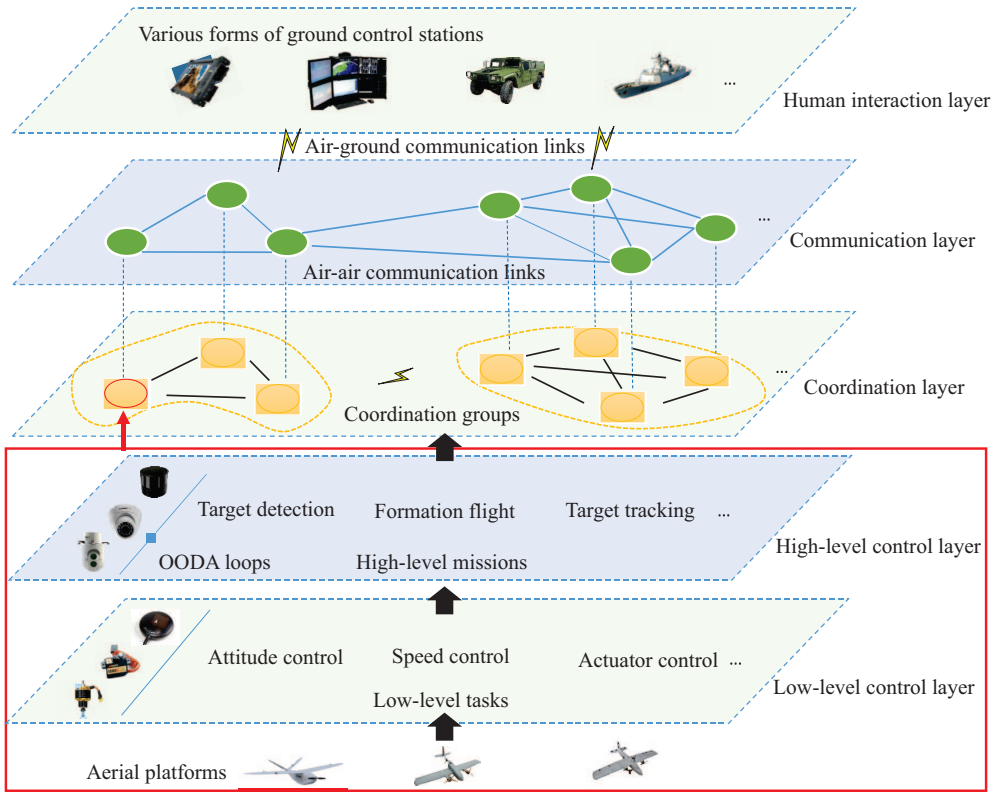


**Figure 3** (Color online) The multi-layered group-based UAV swarm architecture.

## 3 Multi-layered group-based architecture for mission-oriented UAV swarms

The coordination architecture is vital to achieving the desired formation flight of a large-scale UAV swarm. System architectures for multi-UAV coordination have been increasingly investigated in recent years (for example [2, 3]). However, these approaches are designed for small numbers of UAVs without considering their scalability to larger systems. Some recent architectures that have been proposed for large-scale UAV swarms in autonomous flight (such as [29]) neglect the need for mission coordination. This section proposes a multi-layered group-based architecture for mission-oriented swarm systems.

### 3.1 The system architecture

The proposed architecture consists of five layers, as illustrated in Figure 3. The highest level (the human interaction layer) shows the UAV status, the telemetry information, and the geographical environment. It also provides various interaction systems for commanding the swarms. The communication layer deals with message transmission among the UAVs and the control systems. Depending on the mission requirements and the underlying communication availability, the coordination layer dynamically divides the UAVs into several coordination groups. Each UAV within a coordination group shares its status with other UAVs and makes decisions in a distributed manner. The remaining two layers (i.e., the high/low-level control layers) operate at the single-UAV level. Each is included in a single UAV node in the coordination layer. The high-level control layer is deployed on an on-board processing unit and can perform computationally intensive tasks such as path planning, formation control, and target tracking missions. Such high-level missions are accomplished through an observe-orient-decide-act loop. The low-level control layer is deployed on a real-time embedded platform that guarantees minimal system-interrupt latency. This layer executes the low-level control tasks such as attitude and actuator control.

By slicing the swarm system into five layers with specified functionalities, this architecture reduces the complexity of developing a large-scale system. In particular, each layer focuses on its own design and abstracts away the details of other layers. This architecture also divides the UAV swarm into individual

coordination groups, thus restricting the scale of the states maintained on each UAV for decision making as the number of UAVs increases. In this manner, the scalability of the swarm system is significantly improved. Note that our proposed architecture does not depend on the number of UAVs; therefore, the number of UAVs needs not be specified in the system formulation or the control laws. Moreover, our proposed architecture is not restricted to specified kinds of aerial platforms. In fact, based on this architecture, we deploy a swarm of hybrid aerial platforms such as fixed-wing, tilt-rotor, and multi-rotor aircrafts.

### 3.2 Integrated hardware architecture

To design a light-weight and miniaturized system, we propose an integrated architecture for the on-board hardware. The proposed hardware architecture integrates the on-board processing unit, autopilot, perceptional devices, communication payloads, circuitry, and cooling devices into a compact box of weight 450 g and dimensions 108 mm (length)×108 mm (width)×110 mm (height). The hardware architecture contains three layers. The first layer mainly comprises a custom-printed circuit board that distributes the power and provides the wiring interfaces. The second layer mainly comprises an autopilot system that connects to the propulsion system, servos, various sensors, and other equipment. The third layer mainly comprises an on-board processing unit connected to telemetry devices and communication payloads.

### 3.3 Modularized software framework

As mentioned above, each UAV is equipped with an on-board processing unit that effectively executes computationally intensive tasks. On these processing units, we install the Linux system and a robot operating system (ROS). The modularity of ROS enables a modularized software framework for mission-oriented swarm systems. This framework, which corresponds to the high-level control layer in Figure 3, is mainly composed of the following modules.

**Supervision:** The supervision module inspects the status of the system, allows or disallows operations depending on the mission requirements, and manages the communication. This module is essential for ensuring the stability and proper functioning of the system.

**Perception:** This module connects to telemetry devices such as cameras and infrared sensors; moreover, it is responsible for high-level perceptional processing such as target recognition, target localization, and distance detection.

**Orientation:** Based on the information provided by the perception module, the orientation module assesses the current situation, interprets the target's intentions, and detects potential threats. When the predefined conditions are violated, the orientation module triggers the mission planning module for mission execution.

**Mission planning:** The mission planning module produces task plans that satisfy the mission requirements within the imposed constraints such as the UAVs payload, endurance, and airspace regulations. It also negotiates roles and tasks with cooperative UAVs and assigns tasks to the coordination group.

**Guidance control:** This module guides the hosted UAV toward the desired points or issues the command references produced by the mission planning node. In particular, it produces the high-level control references, such as the desired yaw, roll, pitch, speed, and height of the UAV; it sends them to the low-level control layer.

## 4 Coordinated formation flight control

This section presents the overall coordinated-control scheme of the formation flight. The primary processes are the circling rendezvous, formation flight, and pattern reconfiguration, as shown in Figure 4. After take-off, all fixed-wing UAVs implement the consensus-based circling rendezvous mentioned in Subsection 4.1, aiming for alignment. After alignment, the UAVs implement our hybrid formation control proposed in Subsection 4.2, which achieves the desired formation along given paths. During flight, the

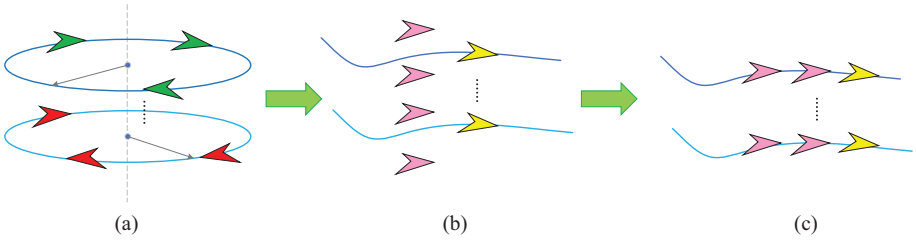


**Figure 4** (Color online) The main processes of coordinated formation flight control. (a) Circling rendezvous; (b) hybrid formation control; (c) formation patter reconfiguration.

formation can smoothly change under our formation pattern reconfiguration technique described in Subsection 4.3. The effectiveness of our proposed methods is corroborated in field experiments. The results are provided in Subsection 4.4.

### 4.1 Consensus-based circling rendezvous

During task executions, a team of UAVs must take off in sequence because the number of runways is limited. Before take-off, each UAV must wait its turn while circling in a prescribed gathering area (i.e., the circling rendezvous). In addition to assisting the forthcoming formation missions, ordered circling is a safety buffer mechanism that greatly reduces the collision possibility among the UAVs in the team.

In our method, the UAVs follow several circular paths of the same radius but at different altitudes. The whole UAV team, denoted by $\Omega$, is divided into $k$ subgroups $\Omega_1, \Omega_2, \ldots, \Omega_k$, where the UAVs in one subgroup have the same altitude. Obviously, $\Omega = \bigcup_{m=1}^{k} \Omega_m$. To form an ordered circling, the subgroups at different altitudes are supposed to reach an angle consensus. Moreover, to avoid collision, all UAVs in the same subgroup are supposed to maintain a certain angular distance (i.e., angular assignment).

These objectives are achieved by the following consensus-based circling algorithm.

(1) Define a coordination variable $\iota_j$ for the whole subgroup $j$:

$$\iota_j = \sum_{i \in \Omega_j} \varphi_i / |\Omega_j|, \tag{1}$$

where $\varphi_i$ denotes the angle between the line pointing from the circle center to UAV $i$ and the north direction.

(2) To assign UAVs in the same subgroup, we sort the UAVs in subgroup $j$ in the ascending order of their errors $|\varphi_i - \iota_j|, i \in \Omega_j$, and obtain the order number $z_i$ for each UAV $i$, where $1 \leqslant z_i \leqslant |\Omega_j|$. The relative angular distance $\varphi_i^r$ with respect to the coordination variable $\iota_j$ is then calculated as follows:

$$\varphi_i^r = \varphi_r \times \left( z_i - \frac{|\Omega_j| + 1}{2} \right), \quad i \in \Omega_j, \tag{2}$$

where $\varphi_r > 0$ denotes the desired angular distance between two neighbor UAVs in the same subgroup.

(3) For coordinated circling, the desired circling velocity of UAV $i$ is calculated as follows:

$$V_i^r = V_c - k_1 \sum_{m=1}^{k} \Gamma(\iota_j - \iota_m)/k + k_2(\varphi_i^r - \Gamma(\varphi_i - \iota_j)), \quad i \in \Omega_j, \tag{3}$$

where $V_c$ denotes the constant cruise speed, $k_1$ and $k_2$ are two scalars, and $\Gamma(x)$ is a regulation function, which is defined as follows:

$$\Gamma(x) = \begin{cases} x, & \text{if } -180 \leqslant x \leqslant 180, \\ x - 360n, & \text{if } -180 + 360n \leqslant x \leqslant 180 + 360n, \end{cases}$$

where $n$ is a positive integer. Protocol (3) is essentially a consensus algorithm. The first item in (3) intends to align all UAVs at different altitudes, and the second item attempts to maintain a constant angular distance $\varphi_r$ during circling of all UAVs at the same altitude.

(a) (b)

**Figure 5** (Color online) Seven UAVs circling in an ordered alignment. (a) Achieving alignment in the ground station; (b) the achieved alignment in the field experiment.

(4) Protocol (3) fails when the UAVs locate evenly on the circling circle. To avoid this undesirable case, we propose a pre-aligning control algorithm that selects a subgroup $L$ as the leader subgroup of the group and aligns the other subgroups to $L$. The pre-aligning control algorithm is described as follows:

$$V_i^r = \begin{cases} V_c + k_2(\varphi_i^r - \Gamma(\varphi_i - \iota_j)), & \text{if } i \in \Omega_j,\ j = L, \\ V_c + k_2(\varphi_i^r - \Gamma(\varphi_i - \iota_j)) + k_3\Gamma(\iota_L - \iota_j), & \text{if } i \in \Omega_j,\ j \neq L, \end{cases} \tag{4}$$

where $k_3$ is the coefficient constant.

The pre-alignment terminates when the condition

$$|\iota_j - \iota_L| < \varphi_t, \quad j = 1, \ldots, k \tag{5}$$

is satisfied, where $\varphi_t$ is a given threshold constant.

The whole process of consensus-based circling is given by Algorithm 1.

**Algorithm 1** Consensus-based circling rendezvous

1: Calculate the angle coordination variable in (1) for each UAV subgroup;
2: **if** all angle coordination variables are sufficiently close to each other, i.e., if Eq. (5) holds, **then**
3: Calculate the desired velocity $V_i^r$ by (3);
4: **else**
5: Calculate the desired velocity $V_i^r$ by (4);
6: **end if**

In Algorithm 1, the angle coordination variable of each subgroup plays two important roles:

• Inner-group assignment. The front angle of all UAVs in a subgroup is aligned to be exactly equal to the angle coordination variable (which is taken as the reference value of the subgroup).

• Inter-group consensus. With the continuous exchange of angle coordination variables, the velocities of the UAVs in the subgroup are adjusted to maintain sufficiently close coordination values.

We claim that the inter-group consensus on the angle coordination value is necessary for ordered circling and for avoiding undesirable oscillations (i.e., this is a necessary condition for convergence). If consensus is nearly achieved, then each UAV receives an angle assignment (line 3 in Algorithm 1); otherwise, each UAV adjusts its velocities to achieve consensus (line 5). The field experiment result of the circling algorithm is shown in Figure 5.

### 4.2 Hybrid formation control

This subsection describes our hybrid formation control framework by which a group of fixed-wing UAVs follows the given paths (generated by waypoints determined by the flight mission) while maintaining the desired formation. These UAVs are divided into several subgroups, each with one or more leaders:

• The leaders are steered by our coordinated path-following control law. Under this law, the leaders cooperate in following their own paths (see Subsection 4.2.1).

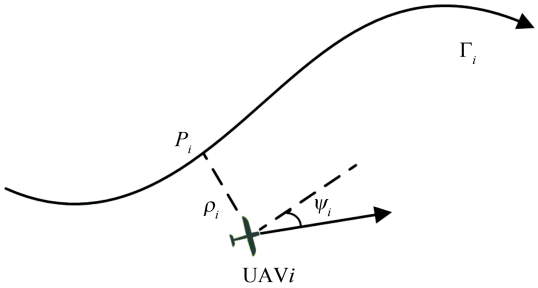


**Figure 6** Description of the path-following problem: point $p_i$ is the projection of the $i$-th leader UAV onto the directed path $\Gamma_i$.

• The followers in each subgroup cooperate with each other in following the group leader(s). This movement is directed by our induced-route-based leader-follower coordination control law (see Subsection 4.2.2).

Note that this hybrid formation-control framework has low communication complexity because the followers (constituting the majority of UAVs) can coordinate without exchanging any path information. Furthermore, the hybrid formation-control framework is scale-independent.

#### 4.2.1 *Coordinated path-following control of the leader UAVs*

Consider that the UAVs move on a 2D plane. The state of the $i$-th UAV is represented as $[x_i, y_i, \theta_i]^{\mathrm{T}}$, where $(x_i, y_i)$ denotes the position of the $i$-th UAV in an inertial coordinate frame, and $\theta_i$ is the orientation of the $i$-th UAV. In this subsection, each UAV model $i$ is simplified as a unicycle model that is governed by the following kinematics:

$$\begin{cases} \dot{x}_i = v_i \cos(\theta_i), \\ \dot{y}_i = v_i \sin(\theta_i), \\ \dot{\theta}_i = \omega_i, \end{cases}$$

where $v_i$ and $\omega_i$ denote the forward and angular speeds of the $i$-th UAV, respectively. In this study, we assume the general case in which the UAVs are subject to input constraints. We impose $0 < v_{\min} \leqslant v_i \leqslant v_{\max}$ and $|\omega_i| \leqslant \omega_{\max}$, where $v_{\max}$ and $v_{\min}$ are the maximum and minimum forward speeds of the UAVs, respectively, and $\omega_{\max}$ is the maximum angular speed.

Following the popular approach, a flight mission is depicted by a set of waypoints, known as the waypoint list. Starting from its current location, each leader UAV must sequentially fly to each waypoint in its waypoint list. Motivated by this requirement, we realized the formation flight through a coordinated path-following approach, in which each leader UAV follows its own path while coordinating with the other leader UAVs. Through this coordination, the leader synchronizes the distance between its projection point on the path and the waypoint corresponding to the desired position of the formation pattern. One path is generated for each leader UAV. To reconstruct the curved paths of typical motion planning missions, we applied curve fitting techniques to the waypoint lists stored by the UAVs.

As shown in Figure 6, we denote $\phi_i = (\rho_i, \psi_i)$ as the path-following error of the $i$-th UAV with respect to its directed path $\Gamma_i$. The error $\rho_i$, called the location difference, indicates the signed distance from the $i$-th UAV's position to its projection $p_i$ on $\Gamma_i$. In particular, $\rho_i > 0$ if the UAV is located to the left of $\Gamma_i$ (with respect to the path direction), and $\rho_i < 0$ otherwise. $\psi_i$ is called the orientation difference, defined as the heading angle of UAV $i$ with respect to the tangent vector of $\Gamma_i$ at point $p_i$. The dynamics of the location and orientation differences are given as follows [30]:

$$\begin{cases} \dot{\rho}_i = v_i \sin(\psi_i), \\ \dot{\psi}_i = \omega_i + \dfrac{\kappa(p_i) v_i \cos(\psi_i)}{1 + \kappa(p_i)\rho_i}, \end{cases}$$

where $\kappa(p_i)$ is the signed curvature of $\Gamma_i$ at $p_i$. Under our path-following control law, the path-following error $\phi_i$ of each leader UAV converges to zero; i.e., each leader can successfully follow its path.

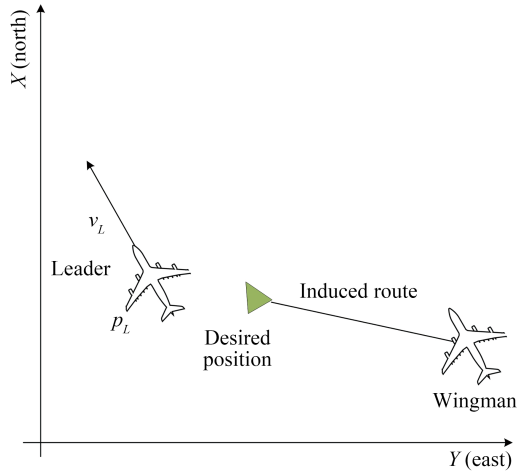


**Figure 7** (Color online) Direct induced route. The position and velocity of the leader are denoted as $p_L$ and $v_L$, respectively.

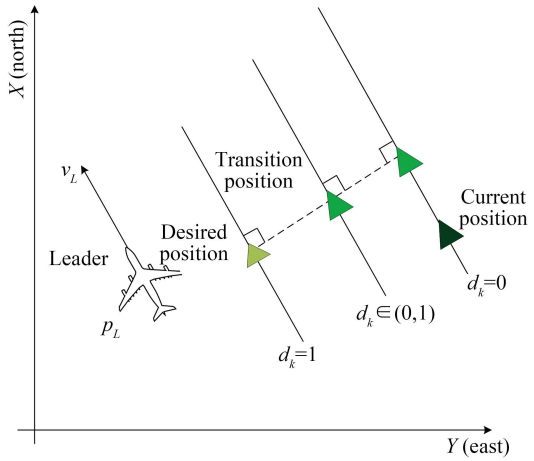


**Figure 8** (Color online) Parallel induced route. $d_k$ is a self-adapted parameter.

In addition to following their own paths, all leader UAVs must simultaneously arrive at their next waypoints. This is achieved by coordination with their neighbors, and is characterized by synchronizing the destination arc distance $\ell_i$ of each leader UAV $i$. The destination arc distance refers to the distance along the path from the UAVs projection to the waypoint of the desired formation pattern. We now propose a control law based on an invariant set called the coordination set, which is defined as follows:

$$\mathcal{S}_c = \{(\rho, \psi) : |\rho| \leqslant R_1, |\psi| \leqslant a, |a\rho + R_1\psi| \leqslant aR_1\},$$

where $0 < a < \pi/2$. Within $\mathcal{S}_c$, the coordinated path-following control law for the $i$-th leader is given as follows:

$$\begin{cases} \omega_i = v_i \left[ -\dfrac{k_1}{k_2}(k_1\rho_i + k_2\psi_i + k_3 \sin(\psi_i)) - \dfrac{\kappa(p_i)\cos(\psi_i)}{1+\kappa(p_i)\rho_i} \right], \\ v_i = \dfrac{1+\kappa(p_i)\rho_i}{\cos(\psi_i)}[v_d + \Sigma_{j\in\mathcal{N}_i}(\ell_j - \ell_i)], \end{cases} \tag{6}$$

where $\mathcal{N}_i$ denotes the set of neighbors of leader UAV $i$, $k_1 \gg k_2 > 0$, $k_3 > 1$, $R_1k_1 - ak_2 < 0$, and $v_d$ is the desired speed of the formation.

Applying the law (6), we use the attitude effects to guide the UAVs toward their projection points on their respective paths. Furthermore, we use the forward speed to coordinate the projection points. When a UAV is outside the coordination set, i.e., the path-following error is large, we apply the single-agent level path-following control law, which returns the UAV to the coordination set. In this case, the UAV focuses on its own path-following mission, ignoring the other UAVs. Once all the UAVs have entered the coordination set, they cooperate with each other to coordinate the path following. We can theoretically prove that all leader UAVs will move in a synchronized manner along their own paths at the desired forward speed. The theoretical proof of the convergence and the detailed analysis of the coordinated path following control laws can be found in [31].

#### 4.2.2 *Leader-follower coordination control of follower UAVs*

In a coordinated mission, the leader UAVs fly along the coordinated path under the control laws elaborated in Subsection 4.2.1. This subsection describes the induced-route-based leader-follower coordination control law, which guides the follower UAVs.

Let $p_L = (x_L, y_L)$ denote the position of the leader UAV, and let $\theta_L$ and $v_L$ denote the yaw angle and velocity of the leader UAV, respectively. The position and yaw angle of the follower (wingman) UAV are denoted by $p_W = (x_W, y_W)$ and $\theta_W$, respectively. The desired position of the follower in the formation is

denoted by $(x_e, y_e)$. When a wingman UAV follows the leader UAV and attempts to join the formation, it first generates a route based on its distance from the desired position. To summarize, the algorithm is a hybrid control algorithm as the generated induced route depends on the wingmans position. In particular, the induced route has two forms determined by the distance between the wingman and the leader UAV: (i) When the wingman is distant from the desired position, the induced route is the line segment from the wingmans current position to the desired position (see Figure 7); (ii) when the wingman is near the desired position, the induced route is the line segment parallel to the leader UAV's trajectory (see Figure 8).

Obviously, the first form of induced route is determined by $(x_e, y_e)$ and $(x_W, y_W)$. The second form can be determined from two points $(x_1, y_1)$ and $(x_2, y_2)$, as described below:

$$\begin{cases} x_1 = x_W + d_k(x_e - x_W), \\ y_1 = y_W + d_k(y_e - y_W), \end{cases} \tag{7}$$

$$\begin{cases} x_2 = x_1 - \delta \sin(\theta_L), \\ y_2 = y_1 + \delta \cos(\theta_L), \end{cases} \tag{8}$$

where $\delta$ is the forward distance and $d_k$ is a self-adapted parameter. As indicated by (7) and (8), the induced route passes through the current position of the wingman when $d_k = 0$, and through the desired position when $d_k = 1$. Obviously, the parameter $d_k$ increases from 0 to 1 as the wingman airplane approaches the desired position. In the field experiment, we selected $d_k = \frac{1}{1+k_g D_e}$, where $D_e = \sqrt{(x_e - x_W)^2 + (y_e - y_W)^2}$ and $k_g$ is a constant coefficient.

We now define a binary variable $\kappa$ for the two forms of induced route. $\kappa = 1$ and $\kappa = 2$ indicate that the wingman follows the first and second form of the induced route, respectively. The induced route switches by a relay-like method depending on the relative distance between the wingmans position $(x_W, y_W)$ and the desired position. The switching is as follows:

$$\kappa = \begin{cases} 1, & \text{if } D_e > r_{\max},\ \kappa = 2, \\ 2, & \text{if } D_e < r_{\min},\ \kappa = 1, \end{cases} \tag{9}$$

where $r_{\max} > r_{\min} > 0$.

As the induced route is being generated, the wingmans path is guided by a guidance law, which is similar to the PLOS guidance algorithm [32]. The desired yaw angle $\theta_d$ of the wingman is then given by the following equation:

$$\theta_d = k_\theta(\theta_e - \theta_W) + k_d d_v + k_\omega \dot{\theta}_L,$$

where $d_v$ denotes the vertical distance between the wingman and the induced route, and $\dot{\theta}_L$ denotes the angular velocity of the leader UAV. $k_\theta$, $k_d$, and $k_\omega$ are constant coefficients, whereas $\theta_e$ is defined by the following equation:

$$\theta_e = \begin{cases} \arctan(y_L - y_W, x_L - x_W), & \text{if } \kappa = 1, \\ \arctan(y_2 - y_W, x_2 - x_W), & \text{if } \kappa = 2. \end{cases}$$

The velocity of the wingman is adjusted based on its position relative to the desired position. The desired velocity $v_d$ is calculated as follows:

$$\begin{aligned} v_d &= v_L + k_1 d_p + k_2 v_{Lg}, \\ d_p &= (y_e - y_W)\cos(\theta_L) + (x_e - x_W)\sin(-\theta_L), \\ v_{Lg} &= v_L \cos(\theta_L - \theta_e) - v_W \cos(\theta_W - \theta_e), \end{aligned}$$

where $d_p$ denotes the projected distance of the wingman from its desired position on the induced route, $v_{Lg}$ denotes the projected velocity error of the wingman from the leader UAV on the induced route, and $k_1$ and $k_2$ are constant coefficients. Once the desired yaw angle $\theta_d$ and velocity $v_d$ are obtained, they are inputted to the lower-level controller.

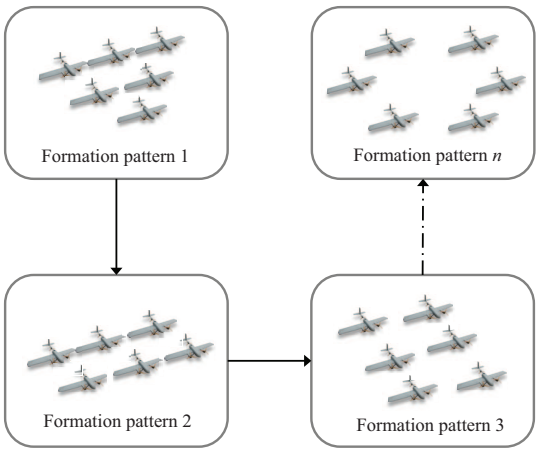


**Figure 9** Formation pattern reconfiguration of a UAV swarm.

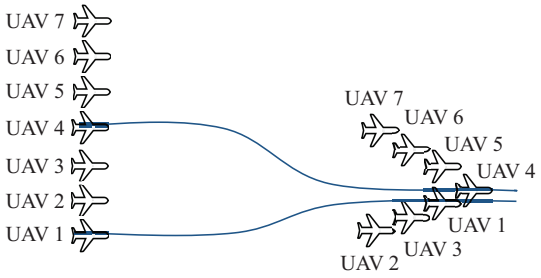


**Figure 10** Formation pattern reconfiguration of a 7-member subgroup of a UAV swarm.

It should be mentioned that the algorithms in Subsection 4.2.2 are inspired by [33] with modifications. The detailed analysis of the convergence of the algorithms will be provided in future work.

#### 4.2.3 *Hybrid formation flight control system*

In the overall hybrid formation control system, one UAV can act as a leader or a follower (or frequently change its role between a leader and a follower) as required by the mission. The on-board algorithm executed by each UAV is summarized in Algorithm 2.

**Algorithm 2** Hybrid formation flight control for UAV $i$

1: **if** UAV $i$ is a leader, **then**
2: Conduct the coordinated path-following algorithm described in Subsection 4.2.1;
3: **else**
4: Conduct the leader-follower coordination algorithm in Subsection 4.2.2;
5: **end if**

The stability of the overall hybrid formation control algorithm can be proven by the input-to-state stability technique. Here, the whole system can be regarded as several cascade systems between the leaders and the followers. Furthermore, it is worth emphasizing that the hybrid formation control system is reasonably robust against random communication delays, communication losses, and UAV failures. Although the performance deteriorates as the communication delay increases, the system remains stable when the delays are bounded.

### 4.3 Formation pattern reconfiguration

This subsection discusses the changes in the formation patterns, which are handled by formation pattern reconfiguration (see Figure 9).

Based on our proposed formation-control laws in the above subsections, we reconfigure the leader and follower UAVs by different strategies. The leaders are reconfigured by coordinated path planning and following. The followers then change their relative positions to align with their leaders.

Consider the circumstance shown in Figure 10. There are two leaders, UAVs 1 and 4, with two (UAVs 2 and 3) and three (UAVs 5, 6, and 7) followers, respectively. During the reconfiguration process, UAVs 1 and 4 implement the coordinated path under the control law proposed in Subsection 4.2.1, reaching their corresponding relative positions in the new formation pattern. Unlike the leader UAVs, the follower UAVs are not usually pre-assigned their relative positions, but are given the desired formation pattern. The number of positions along this formation equals the number of follower UAVs. In this case, the

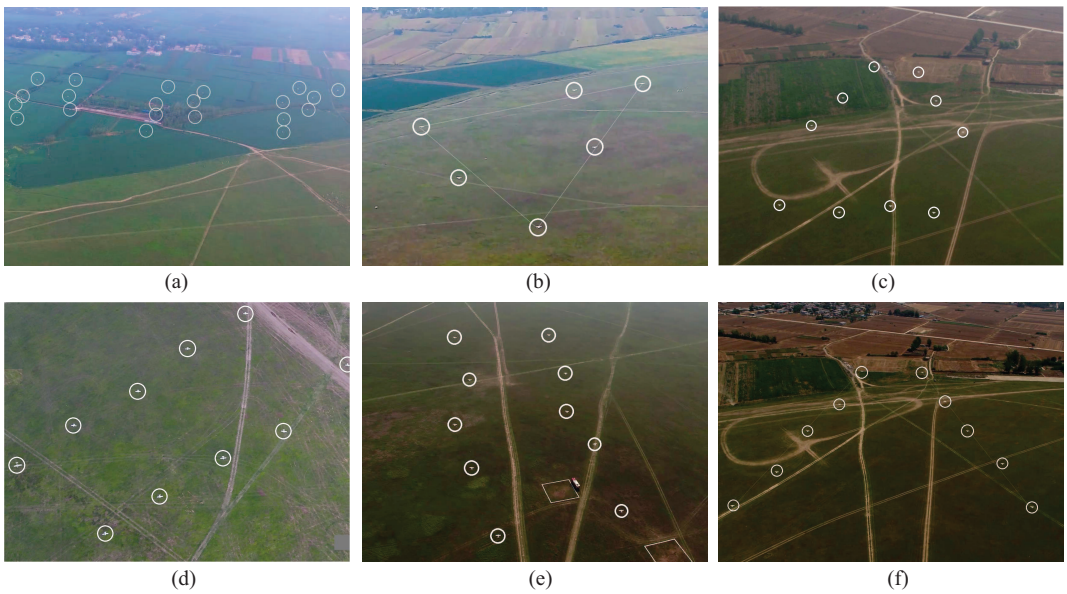


**Figure 11** (Color online) (a) 21 UAV formation; (b) triangle formation; (c) "Ba-Yi" formation; (d) 2-row formation; (e) 2-column formation; (f) V formation.

position assignment of the follower UAVs is optimized by minimizing the worst-case variations in their positions relative to their leader UAV.

Note that the formation pattern reconfiguration is very useful in dealing with the scale change in our multi-UAV system. For instance, when the number of UAVs decreases (by crash or failure), our system will select a new formation pattern and reconfigure it accordingly.

### 4.4 Field experiments of formation flight

The effectiveness of the proposed distributed coordination control laws is evaluated in a series of field experiments using different numbers of fixed-wing UAVs. Typical snapshots of the pattern formations are shown in Figure 11. The hybrid formation control scheme presented in Subsection 4.2 successfully generates and maintains the various pattern formations. Moreover, the patterns are dynamically reconfigured by the strategy presented in Subsection 4.3.

The system performance is analyzed in a formation flight experiment using 21 fixed-wing UAVs. The 21 UAVs are divided into three groups, each with two leaders and five followers (see Figure 12; note that the group number is flexible for a given number of UAVs). Thus, there are six leader UAVs and 15 follower UAVs in total.

The six leader UAVs are governed by the proposed coordinated path-following control law in Subsection 4.2.1. To examine the path-following error, we plot the location and orientation differences in Figures 13 and 14, respectively. The location difference is bounded within $[-10, 10]$ m, and the orientation difference is bounded within $[-0.2, 0.2]$ rad.

We now examine the coordination among the groups. According to our settings, leaders 3 and 4 are required to locate midway between leaders 1 and 5 and between leaders 2 and 6, respectively. The two leaders in Group 1 were 160 m behind the leaders in Group 2 (measured by the distance along the path), whereas the leaders in Group 3 are 160 m in front of Group 2. The group coordination errors of the six leader UAVs are shown in Figure 15. The group coordination error in each UAV is initially large, but gradually reduces to the neighborhood of the origin.

The tracking error of the follower UAVs is investigated in one group as an example. Recall that five followers/wingmen are assigned to each group. The tracking errors of the five follower UAVs (relative to the desired position) are given in Figure 16. The distance errors gradually reduce to small values.

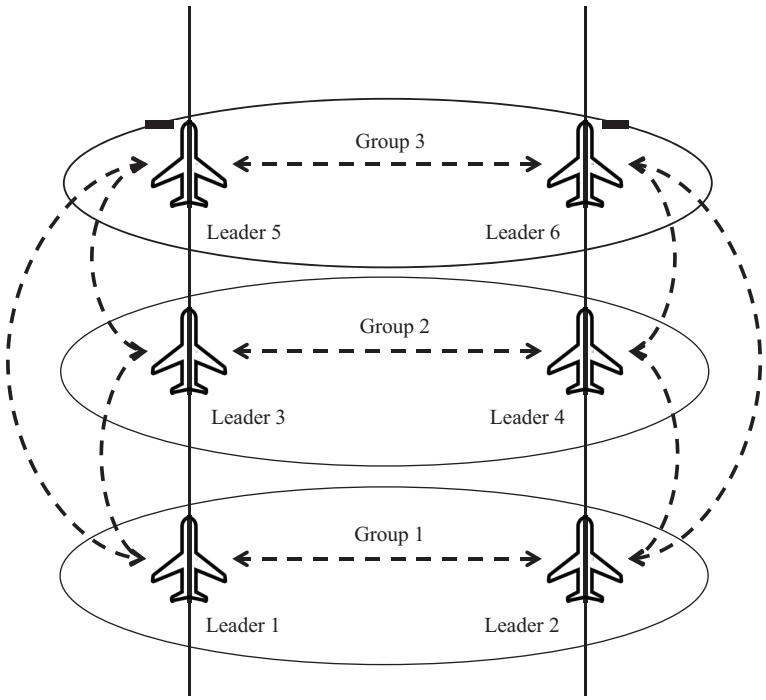


**Figure 12** Demonstration of the path-following settings and communication topology of the six leader UAVs.

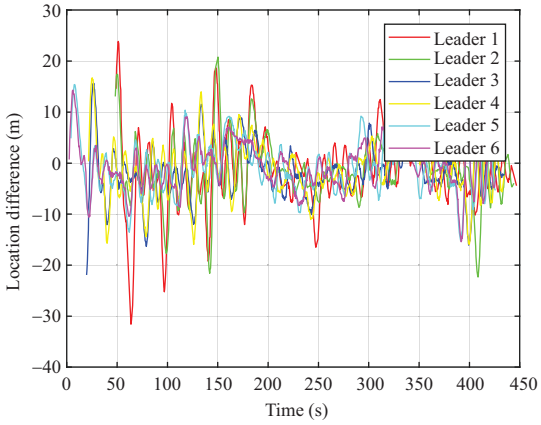


**Figure 13** (Color online) Location differences of the six leader UAVs after entering the coordination set.

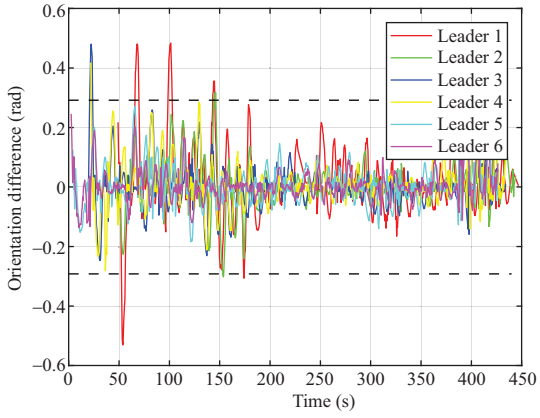


**Figure 14** (Color online) Orientation differences of the six leader UAVs after entering the coordination set.

## 5 Security of UAV formation flight

Security is an important consideration in UAV formation and should be guaranteed in complex environments. Swarms typically encounter two security problems: inter-UAV collisions and obstacles. The first security breach occurs when UAVs fly close to other UAVs in the swarm; the second breach occurs in the presence of obstacles such as uncooperative UAVs, aerostatics, buildings, and mountains.

### 5.1 Inter-UAV collision avoidance

During the course of route tracking, formation flight, and formation reshaping, the trajectories of the UAV in the cluster unavoidably intersect, risking collision among the UAVs. To prevent such collisions, a distributed real-time collision-avoidance algorithm, based on state prediction, is necessitated. The basic idea of the algorithm is explained below.

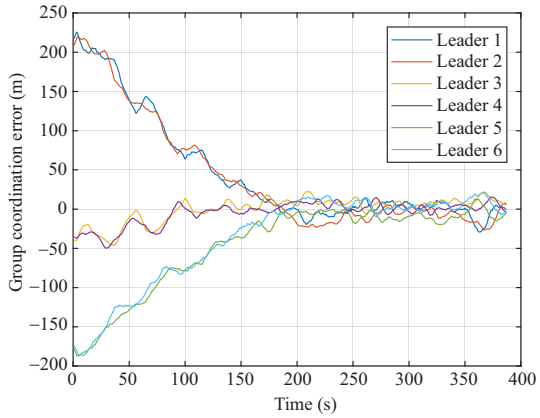


**Figure 15** (Color online) Group coordination errors of the leaders.

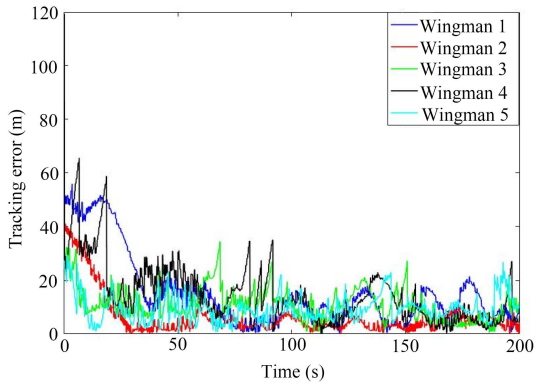


**Figure 16** (Color online) Tracking errors of the five wingmen.

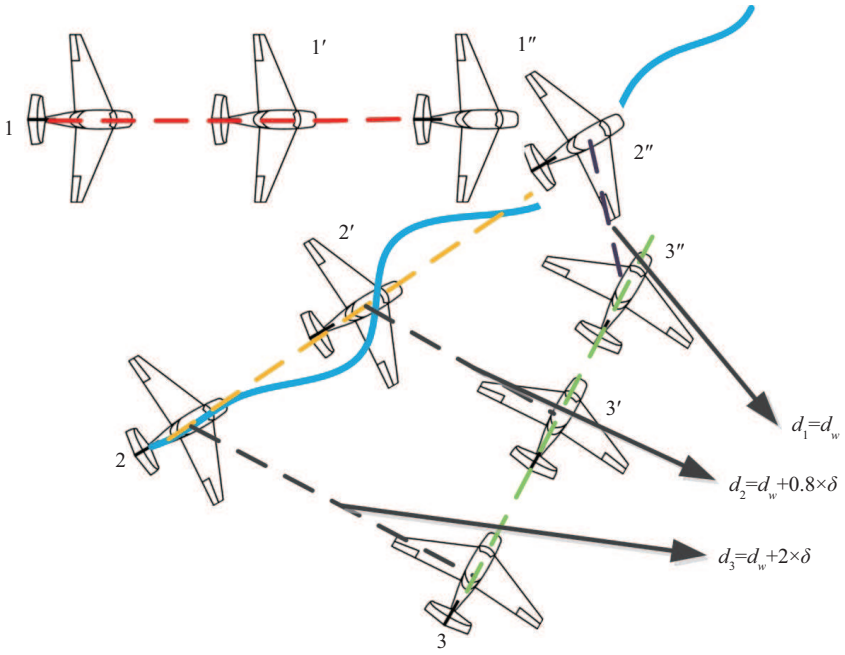


**Figure 17** (Color online) State prediction of the UAVs for collision risk judgment.

- Predict the flight state of the UAVs in the predictive horizon from the current flight-state information of the UAV and its neighbors.
- Judge the risk (high or low) of collision with any specific neighboring UAV.
- Determine the corresponding collision-avoidance maneuver.

Figure 17 shows the state prediction algorithm for collision avoidance, in which $\delta$ represents the prediction step, $d_w$ denotes the wing span of the UAV, and $d_2$ and $d_3$ denote the distances between the UAV and an adjacent UAV in the current moment and the next two prediction horizons, respectively. Collision risk with the adjacent UAV is judged when all three distances ($d_w$, $d_2$ and $d_3$) are shorter than the given thresholds of each time step. If the collision risk is sufficiently high, the algorithm immediately runs the collision avoidance maneuver based on the velocity and heading differences between the potentially colliding UAVs. When the heading difference is large and the velocity difference is small, the maneuver decision adopts a distributed speed-adjustment strategy. When both the heading difference and distance are small, it invokes a distributed heading-adjustment strategy.


**Figure 18** (Color online) Inter-UAV collision avoidance in flight.

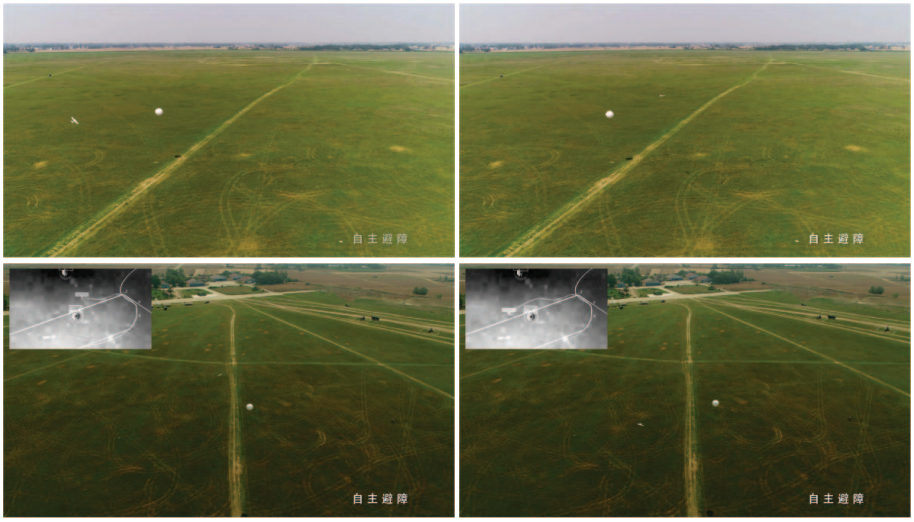


**Figure 19** (Color online) Balloon avoidance in flight tests.

The deployment experiments of 21 fixed-wing UAVs validate the effectiveness of the proposed collision-avoidance strategy. In the flight tests, the inter-UAV collision avoidance method effectively eliminates the collision possibility. The on-board processing unit completes the risk judgment and maneuver decision within 50 ms, and the collision-avoidance maneuver and formation reconfiguration are accomplished within 10 s. Snapshots of inter-UAV collision avoidance during the flights are shown in Figure 18.

### 5.2 Obstacle avoidance

Unexpected obstacles are handled by an obstacle-avoidance strategy based on re-planning. Using the obtained obstacle information, the rapid re-planning algorithm first generates a series of collision-free via-points. The via-points are interpolated by the cubic B-spline curve fitting method, establishing a smooth, collision-free path for the UAV. Finally, the UAV tracks the curved path transferred from the geometric path to realize obstacle avoidance. The whole process, i.e., re-planning, curve fitting, and path following, is embodied in the processing unit and performed online.

To validate the effectiveness of the proposed obstacle-avoidance strategy, we place obstacles (balloons and quad-rotors) in the paths of the flight experiments. The obstacle-avoidance strategy effectively eliminates the collision possibility. The obstacle avoidance maneuver is completed within a short timeframe.

Snapshots of balloon avoidance in the flights are shown in Figure 19.

## 6 Conclusion

In this study, we presented our recent advances on coordinated control problems of multiple miniature fixed-wing UAVs. We proposed a multi-layered, mission-oriented, and modularized architecture, and developed a novel distributed coordinated-control algorithm. The individual path-following approach in the existing literature excludes the cooperation among the UAVs. The efficacy of the proposed techniques was demonstrated in several field experiments by deploying up to 21 fixed-wing UAVs. We successfully produced various formation patterns (triangular, V-shaped, 2-row, and 2-column formations). The formation pattern reconfiguration and the security issues in formation flight are also considered in the current framework. Our proposed method completed the risk judgment and maneuver decision within 50 ms for the on-board processing unit; moreover, it accomplished the collision avoidance maneuver and formation reconfiguration within 10 s.

**Acknowledgements** This work was partly supported by National Natural Science Foundation of China (Grant No. 61801494), and Joint Fund of Ministry of Education of China for Equipment Pre-research and Beijing Nova Program (Grant No. 2018047). The authors express their deepest gratitude to the SWARM TEAM of the NUDT. Without their hard work, the flight experiments could not be done.

**References**

1 Giulietti F, Pollini L, Innocenti M. Autonomous formation flight. IEEE Control Syst, 2000, 20: 34–44
2 Gu Y, Seanor B, Campa G, et al. Design and flight testing evaluation of formation control laws. IEEE Trans Contr Syst Technol, 2006, 14: 1105–1112
3 Yang Y, Polycarpou M M, Minai A A. Multi-UAV cooperative search using an opportunistic learning method. J Dyn Sys Meas Control, 2007, 129: 716
4 Qu Y H, Zhang F, Wu X W, et al. Cooperative geometric localization for a ground target based on the relative distances by multiple UAVs. Sci China Inf Sci, 2019, 62: 010204
5 Michael N, Fink J, Kumar V. Cooperative manipulation and transportation with aerial robots. Auton Robot, 2011, 30: 73–86
6 Jin Y, Minai A A, Polycarpou M M. Cooperative real-time search and task allocation in uav teams. In: Proceedings of the 42nd IEEE Conference on Decision and Control. New York: IEEE, 2003. 7–12
7 Xargay E, Kaminer I, Pascoal A, et al. Time-critical cooperative path following of multiple unmanned aerial vehicles over time-varying networks. J Guidance Control Dyn, 2013, 36: 499–516
8 Cichella V, Kaminer I, Dobrokhodov V, et al. Cooperative path following of multiple multirotors over time-varying networks. IEEE Trans Automat Sci Eng, 2015, 12: 945–957
9 Ren W, Beard R W. Distributed Consensus in Multi-vehicle Cooperative Control. Berlin: Springer, 2008
10 Li Z, Duan Z. Cooperative Control of Multi-Agent Systems: A Consensus Region Approach. Boca Raton: CRC Press, 2014
11 Wang X, Zeng Z, Cong Y. Multi-agent distributed coordination control: developments and directions via graph viewpoint. Neurocomputing, 2016, 199: 204–218
12 Liu J W, Huang J. Leader-following consensus of linear discrete-time multi-agent systems subject to jointly connected switching networks. Sci China Inf Sci, 2018, 61: 112208
13 Ma L F, Wang Z D, Han Q-L, et al. Consensus control of stochastic multi-agent systems: a survey. Sci China Inf Sci, 2017, 60: 120201
14 Zhou J L, Yang J Y, Li Z K. Simultaneous attack of a stationary target using multiple missiles: a consensus-based approach. Sci China Inf Sci, 2017, 60: 070205
15 Wang X, Yadav V, Balakrishnan S. Cooperative uavformation flying with obstacle/collision avoidance. IEEE Trans Contr Syst Technol, 2007, 15: 672–679
16 Abdessameud A, Tayebi A. Formation control of vtolunmanned aerial vehicles with communication delays. Automatica, 2011, 47: 2383–2394
17 Liao F, Teo R, Wang J L, et al. Distributed formation and reconfiguration control of vtoluavs. IEEE Trans Contr Syst Technol, 2017, 25: 270–277
18 Zou Y, Zhou Z, Dong X, et al. Distributed formation control for multiple vertical takeoff and landing uavs with switching topologies. IEEE/ASME Trans Mechatron, 2018, 23: 1750–1761
19 Nigam N, Bieniawski S, Kroo I, et al. Control of multiple uavs for persistent surveillance: algorithm and flight test results. IEEE Trans Contr Syst Technol, 2012, 20: 1236–1251
20 Kushleyev A, Mellinger D, Powers C, et al. Towards a swarm of agile micro quadrotors. Auton Robot, 2013, 35: 287–300

21 Dong X, Zhou Y, Ren Z, et al. Time-varying formation control for unmanned aerial vehicles with switching interaction topologies. Control Eng Practice, 2016, 46: 26–36

22 Dong X, Zhou Y, Ren Z, et al. Time-varying formation tracking for second-order multi-agent systems subjected to switching topologies with application to quadrotor formation flying. IEEE Trans Ind Electron, 2017, 64: 5014–5024

23 Dydek Z T, Annaswamy A M, Lavretsky E. Adaptive configuration control of multiple uavs. Control Eng Practice, 2013, 21: 1043–1052

24 Liu H, Dong X, Lewis F L, et al. Robust formation control for multiple quadrotors subject to nonlinear dynamics and disturbances. In: Proceedings of the 14th IEEE International Conference on Control and Automation. New York: IEEE, 2018. 58–62

25 Xargay E, Dobrokhodov V, Kaminer I, et al. Time-critical cooperative control of multiple autonomous vehicles: Robust distributed strategies for path-following control and time-coordination over dynamic communications networks. IEEE Control Syst, 2012, 32: 49–73

26 Bayraktar S, Fainekos G E, Pappas G J. Experimental cooperative control of fixed-wing unmanned aerial vehicles. In: Proceedings of the 43rd IEEE Conference on Decision and Control. New York: IEEE, 2004. 4292–4298

27 Reynolds C W. Flocks, herds and schools: a distributed behavioral model. SIGGRAPH Comput Graph, 1987, 21: 25–34

28 Hauert S, Leven S, Varga M, et al. Reynolds flocking in reality with fixed-wing robots: communication range vs. maximum turning rate. In: Proceedings of the 2011 IEEE/RSJ International Conference on Intelligent Robots and Systems. New York: IEEE, 2011. 5015–5020

29 Chung T H, Clement M R, Day M A, et al. Live-fly, large-scale field experimentation for large numbers of fixed-wing UAVs. In: Proceedings of 2016 IEEE International Conference on Robotics and Automation. New York: IEEE, 2016. 1255–1262

30 Lan Y, Yan G, Lin Z. Synthesis of distributed control of coordinated path following based on hybrid approach. IEEE Trans Automat Contr, 2011, 56: 1170–1175

31 Chen H, Cong Y R, Wang X K, et al. Coordinated path following control of fixed-wing unmanned aerial vehicles. 2019. ArXiv: 1906.05453

32 Kothari M, Postlethwaite I. A probabilistically robust path planning algorithm for UAVs using rapidly-exploring random trees. J Intell Robot Syst, 2013, 71: 231–253

33 Wu J C, Zhou R, Dong Z N, et al. Formation flight control method of multiple UAVs based on guidance route (in Chinese). J Beijing Univ Aeronaut Astronaut, 2016, 42: 1518–1525